J Solid State Electrochem (2005) 9: 259–266
DOI 10.1007/s10008-004-0633-7

ORIGINAL PAPER

Eli Lancry · E. Levi · Y. Gofer · M. D. Levi
D. Aurbach

The effect of milling on the performance of a Mo_6S_8 Chevrel phase as a cathode material for rechargeable Mg batteries

Received: 19 August 2004 / Revised: 4 November 2004 / Accepted: 11 November 2004 / Published online: 24 February 2005

Abstract In the present study, we explored how milling Mo_6S_8 Chevrel phase in inert or air atmosphere affects their electrochemical behavior as a Mg-ion insertion material for rechargeable Mg batteries. Electrochemical tools such as slow scan rate cyclic voltammograms and potentiostatic intermittent titration technique have been used in conjunction with X-ray diffraction, X-ray photoelectron spectroscopy, and electron microscopy. In contrast to the deterioration observed for milling Mo_6S_8 in air, it's milling under Ar results in specific capacity increase due to improved Mg-ion diffusion kinetics. It was shown that in spite of the conservation of the bulk crystallographic structure, both for air and the Ar-milled materials, they differ significantly in the average particle sizes and the degree of surface oxidation state.

Keywords Milling · Mo_6S_8 Chevrel phase · Mg-ion insertion · Rechargeable Mg battery · SSCV · PITT

Introduction

In spite of an expected general similarity between the processes of Li and Mg-ion insertion into inorganic host materials, there is, so far, only very limited selection of intercalation materials for cathodes of rechargeable Mg batteries. In fact, most of the compounds that exhibit fast and reversible Li-ion insertion perform very poorly in Mg^{2+} ions. The insertion of divalent Mg^{2+}, Ca^{2+}, Zn^{2+}, and trivalent Y^{3+} ions into a number of transition metal oxides, phosphates and sulfides, such as Co_3O_4, V_2O_5, $Mg_{0.5}Ti_2(PO_4)_3$, and TiS_2 was reported. However, these cases share common features: they all showed slow kinetics, as well as a low intercalation level, [1–10]. The reason for this relates to the multivalency of the above cations that result in high energetic barriers for solid-state ion diffusion, along with difficulty in the redistribution of the electronic charge in the host, in the vicinity of the ion residing site.

Up to now, only the Chevrel phases, $Mg_xMo_6T_8$(T = S, Se; $0 < x < 2$), exhibit sufficiently fast and reversible Mg^{2+} insertion, that is essential for the development of practical rechargeable batteries. The crystal structure of this family of materials contains octahedral Mo clusters, connected by metallic bonds. This creates, within the Chevrel structure, large "complex" anions containing delocalized electrons [11]. Due to the delocalization of the electrons, these clusters can tolerate easily changes in its electron density, changes of up to four electrons. As a consequence, these clusters are assumed to allow fast redistribution of electrons, needed to maintain local electroneutrality within the host crystal as the insertion of Mg^{2+} ions takes place. Hence, Mo_6S_8 can be considered as an attractive cathode material for rechargeable Mg batteries. This material, however, is thermodynamically unstable, and could be obtained only indirectly by a chemical or electrochemical leaching of a more stable, metal-containing Chevrel phase, e.g., $Cu_2Mo_6S_8$. The high temperature synthesis (1,000–1,200 °C) of the latter compound from the elements or the sulfides in evacuated, sealed quartz tubes is well documented [12, 13].

We have demonstrated the feasibility of utilizing Mo_6S_8 as cathodes in rechargeable magnesium batteries, using Mg anodes (foil), composite cathodes (comprising Mo_6S_8 as the active mass together with carbon and a polymeric binder), and electrolyte solutions composed of ether solvents such as THF and complexes of the stoichiometric formulae $Mg(AlCl_2R_2)_2$, R= –CH_3, C_2H_5, C_4H_9 (Me, Et, Bu). Such cells showed promising performance in terms of the specific capacity around 90–100 mAh g^{-1} (based on

Dedicated to Prof. G. Horanyi on the occasion of his 70th birthday

E. Lancry · E. Levi (✉) · Y. Gofer
M. D. Levi · D. Aurbach
Department of Chemistry, Bar-Ilan University,
52900 Ramat-Gan, Israel
E-mail: levimi@mail.biu.ac.il
Tel.: +972-3-5318832
Fax: +972-3-5351250

the active components), reasonable rates and excellent cycleability [14].

Although so far we have found that the Mo_6S_8 Chevrel phase is the best cathode material for magnesium batteries compared to other hosts, we revealed that Mo_6S_8 does suffer from some kinetic limitations at room temperature [15–17]. This material is able to insert two Mg^{2+} ions per Mo_6S_8 unit upon the first discharge of the electrode, corresponding to a theoretical capacity of 122 mAh g^{-1}. However, not all the intercalated magnesium can be deintercalated at room temperature, resulting in a capacity loss (approximately by 15–20% at room temperature). We investigated these kinetic limitations, which can be considered as charge trapping, and attributed them, at least in part, to the low ion conductivity of $Mg_xMo_6S_8$, at a low level of x. It should be noted that at higher temperatures, these kinetic limitations disappear, e.g., a complete Mg-ion extraction is accomplished upon cycling $Mg_xMo_6S_8$ cathodes at 60 °C (i.e., $0 \le x \le 2$ [15]).

Another possible way of improving the insertion–extraction kinetics of Chevrel phase electrodes could be the reduction of the particle size by milling. It was previously shown [18] that the product of the high temperature synthesis, $Cu_2Mo_6S_8$ (CuCP) is not stable upon milling. The mechanical treatment of the latter compound leads not only to an unusual amorphization, but also to a chemical reaction in which the Cu^+ ions are reduced and removed from the CuCP lattice, in concert with Mo oxidation to MoS_2 [18]. It has been shown that this unusual instability of CuCP to milling leads to a drastic decrease in battery performance.

The aim of this work was to avoid the undesirable reactions obtained by the mechanical treatment of the CuCP cathode materials, by milling the *leached* product, Mo_6S_8. We examined the influence of milling Mo_6S_8 particles, both in inert atmosphere (pure Ar) and air, on their performance as the active mass for Mg-ion insertion electrodes.

Experimental section

The Chevrel phase compound of the $Cu_2Mo_6S_8$ composition was synthesized by a reaction of the palletized powdered elements mixture in evacuated, sealed quartz tubes. The procedure consisted of four sequential stages:

1. Heating at 450 °C for 24 h
2. Heating at 700 °C for 24 h
3. Heating at 1,050 °C for 48 h
4. Cooling down to room temperature at a rate of 120 °C/h.

Cu was extracted from the synthetic product $Cu_2Mo_6S_8$ in a 6 M HCl /H_2O (1:1) solution under air atmosphere (O_2 is the oxidizer).

Milling was performed in air and in the argon atmosphere (glove box) using a Crescent Wig L-Bug Amalgamator (Model 3110B). Powdered Mo_6S_8 (0.5 g) and a steel ball (6.35 mm in diameter) were placed in a cylindrical stainless steel vial (2 cm^3). The weight ratio between the steel ball and the powder was 2:1. In this grinding machine, the ball hits the powder particles, thus producing shock interactions. The morphology of the Mo_6S_8 powders was characterized by scanning electron microscopy (SEM), JSM-840 from JEOL Inc.

The electrochemical behavior of the Mo_6S_8 electrodes was studied using a computerized Arbin Inc. (USA) multichannel battery tester. The electrodes were prepared as follows: the active mass mixture (about 5 mg of Mo_6S_8 + 10% carbon black + 10% PVdF) was spread on a 1×1 cm^2 stainless steel mesh, as already described [15–17]. These electrodes were measured in galvanostatic and voltammetric experiments. The electrolyte solutions used, comprising 0.25 M $Mg(AlCl_2BuEt)_2$ in THF (DCC/THF), were prepared as already described [19]. Strips of Mg foil served as counter and reference electrodes.

X-ray diffraction (XRD) studies were performed with a Bruker Inc. (Germany) AXS D8 ADVANCE diffractometer (Cu Kα radiation). Measurements of the particles' surface area were carried out using a Micrometrics Inc. Gemini 2375 model surface analyzer (nitrogen adsorption/desorption isotherms) according to the Brunauer-Emmett-Teller, (BET), approach. Surface studies of the pristine and milled powders were performed by X-ray photoelectron spectroscopy (XPS) (Kratos Inc., England, Axis HS spectrometer).

Results and discussion

Cyclic voltammetry studies of the effect of milling Mo_6S_8 particles in conjunction with their characterizations by XRD and SEM

Figure 1 shows the XRD peak related to the 101 planes of a pristine Mo_6S_8 powder and that of the milled materials for different periods of time (from 1 to 15 min), under pure Ar atmosphere or in air (a and b, respectively). It is seen that in both cases, the peaks re-

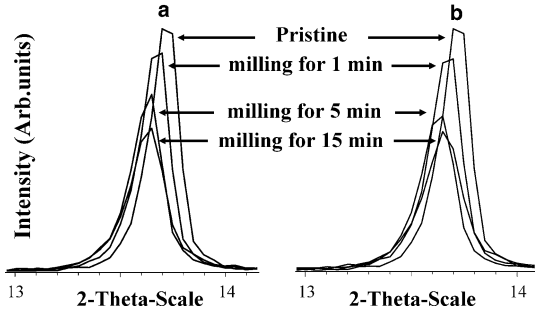

Fig. 1 The 101 peak in XRD patterns of a pristine Mo_6S_8 sample and in XRD patterns of Mo_6S_8 samples milled for different periods of time (from 1 min to 15 min as indicated) in pure Ar atmosphere and in air (**a** and **b**, respectively)

lated to the milled materials shift to lower values of 2θ, their intensity decreases and the peaks become broader as the duration of the milling is longer. Thus, grinding the pristine Mo_6S_8 particles results in the same deterioration of the pristine bulk crystal structure (amorphization and a decrease in the crystallite size) for the air and Ar milled samples.

The effect of grinding on the particles' morphology was further studied by SEM. Figure 2 presents micrographs obtained for pristine samples (a) and milled in Ar (b–d) and in air (e–g). As can be seen, the average size of the particles decreases with milling time. In addition, an aggregation of the extensively ground particles is seen for the samples milled in air for 15 min (Fig. 2g).

Figure 3 shows the specific surface area of the pristine and ground samples (obtained by BET), as a function of grinding time and operation conditions (atmosphere). Whereas grinding in Ar results in a progressive increase in the surface area of the samples (from 5 $m^2\ g^{-1}$ to 16 $m^2\ g^{-1}$), milling in air leads to a moderate increase, reaching a plateau after 5 min of milling (see Fig. 3). The latter feature is certainly in line with the SEM measurements that showed that prolonged grinding in air results in the aggregation of the small (ground) particles.

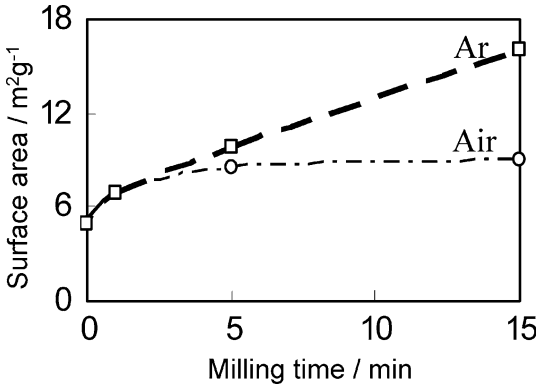

Fig. 3 The dependence on milling time of the specific surface area of Mo_6S_8 samples milled in pure Ar and in air, obtained by the BET method

Figure 4a and b show slow scan rate cyclic voltammograms (SSCVs) ($v = 25\ \mu V\ s^{-1}$) for a pristine Mo_6S_8 electrode and for electrodes comprising milled Mo_6S_8 samples for the different periods of time in Ar and air atmosphere (a and b, respectively). Both families of SSCV curves are comprised of two redox-peaks (a/a′ and b/b′, the first cathodic peak "a" appears as a shoulder at high scan rates), reflecting the consecutive insertion of the first and the second Mg-ions into the Mo_6S_8 host. This results in separate phases, $Mg_1Mo_6S_8$ and $Mg_2Mo_6S_8$, respectively (a detailed discussion of the related phase diagram and the electroanalytical features of SSCV responses has been presented elsewhere [15]). Our current interest is concentrated just on the dependence of

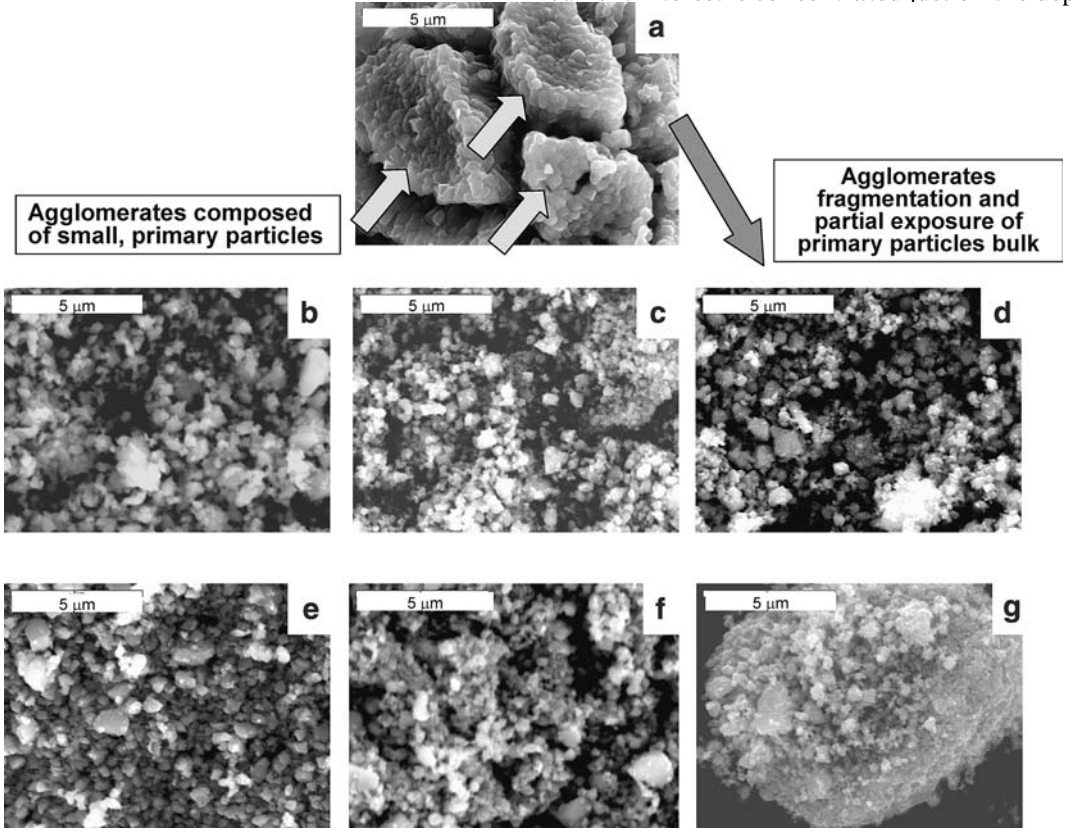

Fig. 2 SEM micrographs of pristine (**a**) Mo_6S_8 powder and powders produced by milling in pure Ar (**b–d**) and in air (**e–g**) for 1, 5 and 15 min, respectively

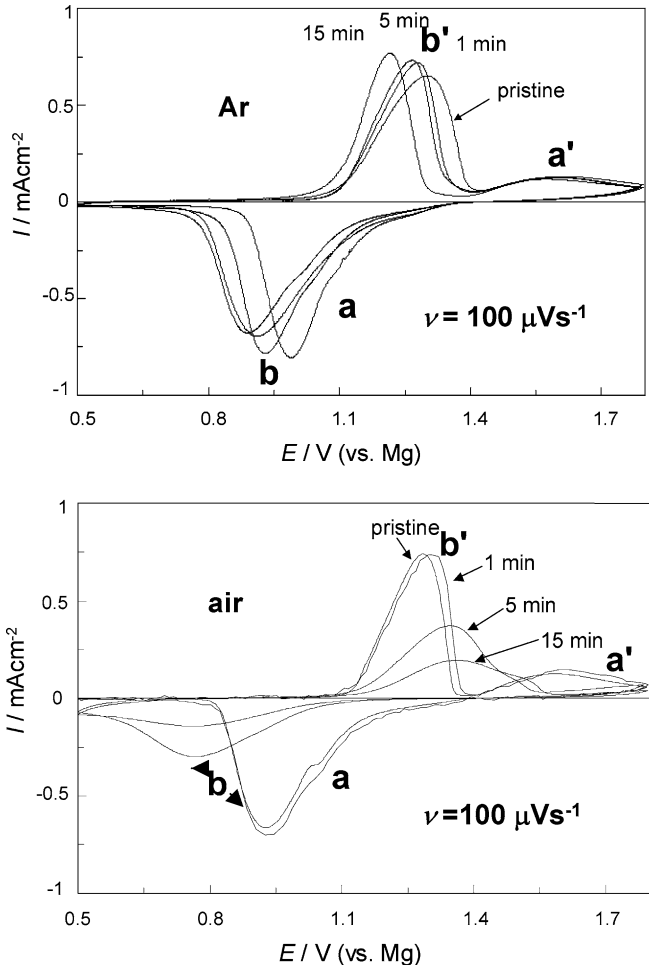

Fig. 4 SSCV curves measured from an electrode comprising a pristine Mo_6S_8 Chevrel phase and from electrodes comprising the Mo_6S_8 active mass, milled in pure Ar (**a**) and in air (**b**) during 1, 5, and 15 min, as indicated. Redox peaks a/a′ and b/b′ relate to $Mo_6S_8|Mg_1Mo_6S_8$ and $Mg_1Mo_6S_8|Mg_2Mo_6S_8$ phase transitions

the SSCV response on the milling time of the active mass and on the operation conditions. From Fig. 4a and b it is seen that the milling substantially affects the intercalation kinetics (mainly, the rate of the solid-state diffusion of the intercalated Mg-ions, reflected by SSCV peak widths), but in a manner that greatly depends on the atmosphere in which the milling was performed. Whereas the intercalation kinetics becomes pronouncedly more facile with the milling time in Ar (note the peak potential separations and the peak widths on the voltammetric curves in Fig. 4a), an opposite trend is observed for the case of the air milled samples: the peaks become broader and their potential separations increase with milling time, which is indicative of the deterioration of the intercalation kinetics (Fig. 4b).

The effect of grinding time and atmosphere on the voltammetric behavior of Mo_6S_8 Chevrel phase electrodes, as demonstrated in Fig. 4, may result from the following factors:

1. A decrease in the average size of the particles in contact with the solution as the milling time is longer, which means a shorter diffusion length for Mg^{2+} ions in the host and higher surface area, resulting in a decrease of the diffusion resistance
2. The milling process creates new surfaces. These surfaces originate from the bulk—parts of the material that was not exposed before to the ambient. Now, depending on the milling atmosphere, these surfaces would possess different chemistry, and thus properties, such as electronic and ionic conductivity
3. Partial amorphization of the particles (especially in long milling periods), which is expected to result in the deterioration of the intercalation kinetics; Mg intercalation kinetics is very sensitive to the crystallography of the host, and, as was mentioned above, it is the Chevrel phase that possesses the best kinetics.

The improvement of the intercalation kinetics when the Mo_6S_8 particles are milled in Ar atmosphere (Fig. 4a) appears to originate from the dominance of the first two factors (1 and 2). The deterioration of the intercalation kinetics when the active mass is milled in air (Fig. 4b) is presumably caused by last two factors (2 and 3). These assumptions were proved by a careful analysis of the diffusion kinetics for pristine and milled samples (in Ar atmosphere) and XPS characterizations of the samples milled in Ar and in air. Note that in spite of the progressive kinetics improvement for the samples milled in Ar, the specific capacity changes are more complicated: a maximal capacity was obtained for the materials after 5 min of milling. In fact, after 15 min of milling in Ar, the material reveals faster kinetics but lower capacity due to the general loss of the active mass (amorphization).

Diffusion kinetics for Mg-ions insertion into milled and unmilled Mo_6S_8 studied by the potentiostatic intermittent titration technique (PITT)

We start with the consideration of the diffusion kinetics. The differential intercalation capacitance, $C_{dif}(E)$, and the characteristic diffusion time constant, $\tau_{dif}(E)$, were calculated based on the theory of PITT, i.e. on the analysis of amperometric responses of the electrodes to small potential steps perturbations [20–22]. The first quantity is defined as the ratio between the charge injected during a potential step (ΔQ) and the height of this potential increment (ΔE):

$$C_{dif}(E) = \frac{\Delta Q}{\Delta E}, \quad (1)$$

where ΔQ can be obtained by the numerical integration of the relevant I versus t curve. The $C_{dif}(E)$ is an important equilibrium characteristic of the intercalating host.

The diffusion time constant τ_d is obtained from the Cottrell domain, identified in the amperometric response of the electrodes (I versus t, $t << \tau_d$) [20–22].

The potential dependence of τ_d related to the short-time Cottrell domains of the chronoamperometric curves can be conveniently calculated using a simple expression [22]:

$$\tau_d(E) = \left[\frac{C_{dif}}{\pi^{1/2} I t^{1/2}/\Delta E}\right]^2, \quad (2)$$

where $It^{1/2}/\Delta E$ is the characteristic, time-independent parameter that characterizes the Cottrell domains of the I versus t curves. The chemical diffusion coefficient $D(E)$ in a spherical electrode particle of a radius r (rough approximation of real particles) is calculated according to the simple expression:

$$D(E) = r^2/\tau_d(E). \quad (3)$$

Simplifying the model for spherical particles, it is assumed that the characteristic diffusion length r (taken as the sphere's radius) is independent of the potential, but is obviously a function of the milling time). Thus, $D(E)$ should be independent of r (and hence it does not depend on the milling time), in contrast to the values of $\tau_d(E)$ (see Eq. 3). It is important to realize that the latter conclusion is correct only if the average electrode particle size changes with the milling time, without changing their bulk properties (in particular, the crystal structure), which may completely change the electrochemical behavior of the material.

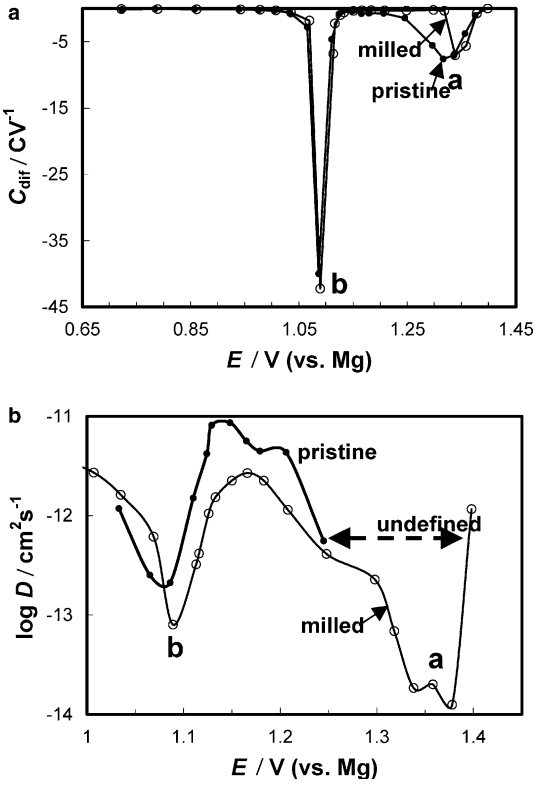

Fig. 5 The potential dependence of the differential intercalation capacitance, C_{dif} (**a**) and the chemical diffusion coefficient, D (**b**) for electrodes comprising pristine and milled (Ar atmosphere, 5 min), Mo_6S_8 powder, calculated from the PITT measurements

Figure 5a, b shows the potential dependence of C_{dif} and D for electrodes containing pristine Mo_6S_8 and Mo_6S_8particles milled for 5 min under Ar atmosphere, respectively. As was mentioned above, C_{dif} obtained from PITT measurements (Eq. 1) reflects almost equilibrium conditions of intercalation and deintercalation, in contrast to the similar quantity obtained from SSCV: $C_{dif} = I/v$ [22]. A comparison between the curves shown in Figs. 5a (PITT) and 4a, b (SSCV) shows that even at slow scan rates, the SSCV curves do not reflect equilibrium conditions of intercalation–deintercalation processes, as is the case for PITT measurements [22] (e.g., compare the width of the peaks in Figs. 4a and 5a). This is because SSCV is a large-amplitude technique, and thus the C_{dif} versus E curves obtained by this technique demonstrate broader peaks for the intercalation processes occurring via first-order phase transitions (distortions due to large Ohmic drops and limitations due to new-phase nucleation and solid-state diffusion), compared to that obtained by PITT [22]. Figure 5a provides sufficient information to compare the C_{dif} versus E responses from pristine and milled samples. A pronounced difference was noted only for the couple a/a′ (see the relevant voltammetric peaks in Fig. 4, related to the initial magnesiation–demagnesiation): the peak related to the milled sample is much narrower than that for the pristine one.

The consequence of the above difference on the width of peak "a" becomes even more pronounced when analyzing log D versus E plots (Fig. 5b). The calculation of D for electrodes comprising pristine and milled materials using Eqs. 2 and 3 depends, of course, on the choice of the value of r. As follows from Fig. 2, milling Mo_6S_8 particles in Ar results in a complete separation of the aggregates (seen only in the SEM micrograph of the pristine sample, Fig. 2a) into smaller, individual particles. We do not know, however, if FWHM of the particles' size average could be assigned correctly to the characteristic diffusion length r for the electrodes containing pristine Mo_6S_8 particles, since the *real* porous structure of the aggregates (characterizing the morphology of this active mass) was not studied. Hence, we used effective values of r calculated from the following simple equation, which is valid for particles of spherical shape:

$$r = \frac{3}{\rho A}, \quad (4)$$

where ρ is the density of a non-porous Mo_6S_8 mass (equal to 5.2 g cm^{-3}), and A denotes the specific surface area of the samples as determined by BET (see Fig. 3). From these data, the average value of r of the pristine sample was found to be 0.5 μm, whereas that after 5 min of milling in Ar the average radius of the particles (i.e.,

the assumed diffusion length) becomes twice as low, i.e., 0.25 μm. These values of r were used in Eq. 3 for the calculation of the D versus E plots shown in Fig. 5b, and, as seen from this figure, the shape of the peak b is generally similar for both the samples. Much more interesting and reliable is the qualitative difference in the electroanalytical behavior of both electrodes around peak a. We were unable to detect Cottrelian regions around this peak for the electrodes comprising pristine Mo_6S_8.

In order to better understand the reason for the absence of the Cottrelian behavior around the potentials related to the first-magnesiation/last-demagnesiation process (peak a) for pristine Mo_6S_8, we compare in Fig. 6a, b whole sets of I versus t curves obtained during potentiostatic titrations of both electrodes (comprising pristine and milled materials). Whereas the shape of the current transients is qualitatively very similar for both electrodes in the vicinity of peak b (monotonous decrease of current with time), a drastic difference was observed for the current transients around peak a. In Fig. 6b, it is clearly seen that the transient current *increases* with time at the potential 1.335 V (versus Mg), whereas we failed to find a similar feature on the current transients of the milled sample (Fig. 6a, see also the inset in this figure). An increase in the transient current with time during a potential step of small amplitude was previously ascribed to a slow nucleation rate during a first-order phase transition, which was nicely demonstrated for the lithiation processes of $Li_xMn_2O_4$ spinel [23] and graphite [24]. Hence, grinding the pristine Mo_6S_8 sample in Ar atmosphere results in an increase of the nucleation rate of $Mg_1Mo_6S_8$ in the bulk of the Mo_6S_8 phase. This effect cannot be explained entirely by the decrease in r as a result of milling. Although a decrease in the diffusion time constant for the Mg-ions in the milled samples, compared to that for the active mass, may be responsible for the higher concentration of nucleation centers in the former electrode, we believe that the grinding process in Ar atmosphere also causes opening of the surface structure of pristine particles. Surface electronic conductivity of thus milled samples appears to be higher than that of the pristine one because the latter contains more oxygen, as is shown below from the XPS characterizations.

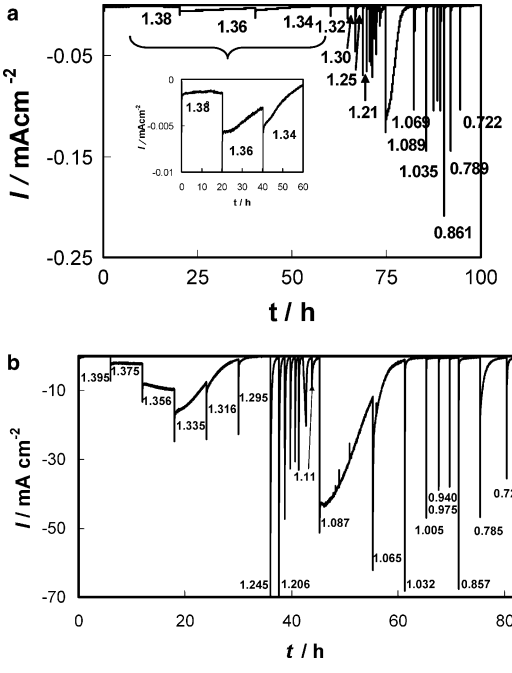

Fig. 6 Complete sequences of transient current–time plots obtained by the potentiostatic titrations of electrodes comprising Mo_6S_8 powder milled in air (5 min) (**a**), and pristine powder (**b**). The potentials during the titrations are indicated. The inset in Fig. 6a shows in more detail the potential domain in which initial magnesiation takes place

XPS characterization of Mo_6S_8 particles ground in Ar and air

In order to clarify the impact of the atmosphere, in which grinding was performed, on the kinetics of the initial magnesiation of the Mo_6S_8 phase, XPS spectra were measured from samples milled in Ar and in air (see Fig. 7a, b, respectively). The Mo 3-D spectra of the Ar–Mo_6S_8 phase show the evolution of Mo at a higher oxidation state with milling time. The presence of this species is obvious in the spectrum of the sample milled for 15 min, but a slightly larger FWHM of the peaks related to the sample milled for 5 min reflects the presence of this type of Mo atoms in the samples even after 5 min of milling. We attribute the appearance of the Mo in the milled samples (under Ar), as reflected by the appearance of a second Mo peak in the XPS response, to a comproportionation reaction leading from Mo_6S_8 to MoS_2 and MoS.

All the Mo_6S_8 samples milled in air show an additional Mo 3-D peak at ca. 236 eV, probably the 3/2 spin-orbit couple of a 5/2 peak, hidden under the 3/2 of the

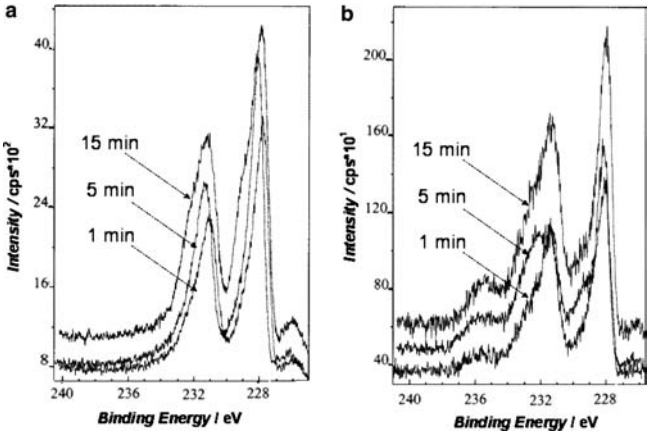

Fig. 7 Mo 3-D XPS spectra of Mo_6S_8 powders milled in Ar (**a**) and in air (**b**) during 1, 5, and 15 min, as indicated

main one (5/2 at ca. 228 eV). This peak grows with milling time. The presence of an oxidized form of Mo is obvious in the 15-min sample that contains a doublet around 231–232 eV. In addition, an evolution of a peak at ca. 229.5 eV, in conjunction to the main peak, is seen with increasing milling time.

The S 2*p* spectra of air-milled Mo_6S_8 samples show an extra feature, as compared to the Ar milled samples, at ca. 169 eV (Fig. 8). This feature grows with milling time. It indicates oxidation of the sulfide anion to sulfate, thus suggesting that some Chevrel phase material converts to molybdenum sulfate as a result of the milling in air. From the quantitative XPS data, it seems that milling Mo_6S_8 in air increases significantly the concentration of oxygen-containing groups on the particles' surface. That the presence of these oxygen layers on the milled Mo_6S_8 particles may slow down the charge transfer related to Mg-ions (from solution phase to the host bulk) could be a major reason for a mechanical deterioration of the performance of these electrodes, as is clearly reflected by the SSCV curves in Fig. 4b.

In fact, interesting information comes from the charging effect, common in XPS analysis of insulators and semiconductors. When the various milled and pristine powder samples were analyzed by XPS we made use of the peak of adventitious carbon as an internal standard for energy scale calibration. Interestingly, there was a trend in the state of the charging, that showed that the pristine sample charged more than that milled in Ar material, which suggests that either the surface, or bulk electronic conductivity of the former one is lower than the latter ones. This is in good agreement with the above suggestion about the opening of clean surfaces from the pristine sample's bulk when milled in Ar. The increase in the surface electronic conductivity of the Ar-milled samples results in the corresponding improvement of their initial (final) magnesiation (demagnesiation) compared to that of the pristine sample. It was found also that the charging effect in the air-milled material increased with milling time, and in all cases was larger than that for the Ar-milled samples.

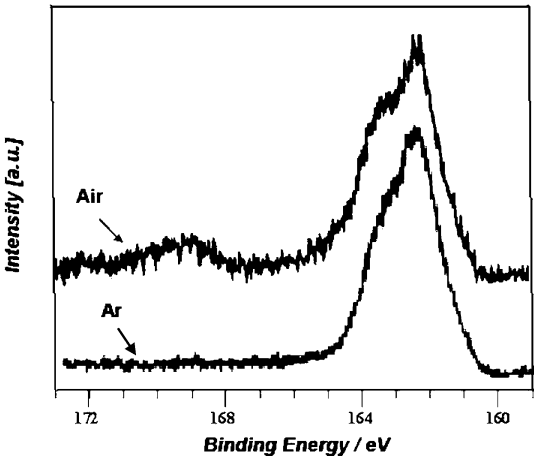

Fig. 8 S 2*p* XPS spectra of Mo_6S_8 powders milled in Ar and in air during 15 min

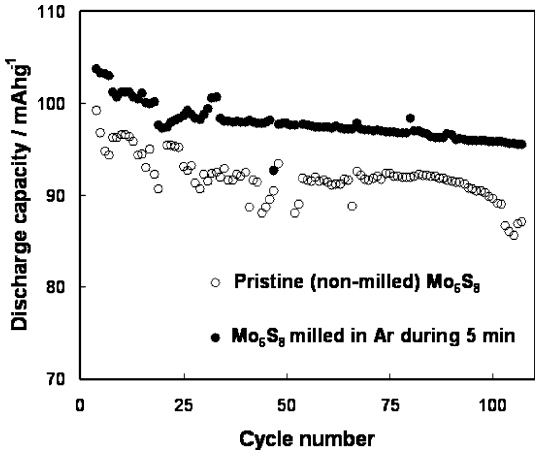

Fig. 9 Discharge capacity of $Mg_xMo_6S_8$ cathodes ($0 < x < 2$) versus cycle number measured during prolonged galvanostatic cycling of prototype rechargeable magnesium batteries. Coin-type cell configuration Mg foil anodes, a THF/0.25 ($Mg(AlCl_2EtBu_2)$) electrolyte solution, C/8 rate. The performance of cathodes comprising a pristine active mass and a milled (Ar) active mass is compared, as indicated

Finally, Fig. 9 compares the cycling behavior of electrodes comprising pristine and milled (in Ar) Mo_6S_8 Chevrel phase as their active mass. At C/8, the performance of the electrodes comprising the Ar-milled particles is superior, both in terms of a higher specific capacity and better cyclability, especially during prolonged magnesiation–demagnesiation cycling.

Conclusions

Mechanical grinding of the active mass of intercalation electrodes for application in rechargeable batteries is a frequently used method for reducing the particles' size, which leads to a better electrode performance (higher rate capability and specific capacity). In this work, we examined the effect of milling Mo_6S_8 Chevrel phase on its performance as cathodes for rechargeable magnesium batteries. XRD, SEM, XPS and surface area measurements were used in conjunction with electrochemical techniques. We show an increase in the surface electronic conductivity of the particles obtained from pristine samples by milling in Ar. This may increase the new phase nucleation rate of the slow and problematic first magnesiation process of this material. These changes positively affect the rate capability and the cycleability of cathodes comprising milled Mo_6S_8. In addition, grinding the Mo_6S_8 particles in Ar definitely decreases the average particle size, and hence, the average diffusion length, and thereby decreases the characteristic diffusion time constant. In contrast, milling Mo_6S_8 particles in air causes dramatic changes in the particles' surface chemistry, including the appearance of molybdenum sulfate-containing surface layers. These surface changes slow

down the rate of Mg-ion transfer into the active mass. A partial amorphization of these milled samples may be a second reason for the considerable deterioration in the performance of the electrodes comprising Mo_6S_8 particles milled in air. These two negative factors obviously dominate the decrease of the average particle size for Mo_6S_8 samples milled in air.

Acknowledgements Partial support for this work was obtained by the Israel Science Foundation (ISF), and by ATU Ltd., Israel.

References

1. Pereira-Ramos JP, Messina R, Perichon J (1987) J Electroanal Chem 218:241
2. Gregory T, Hoffman R, Winterton R (1990) J Electrochem Soc 137:775
3. Bruce PG, Krok F, Nowinski J, Gibson VC, Tavakkoli K (1991) J Mater Chem 1:705
4. Novak P, Desilvestro J (1993) J Electrochem Soc 140:140
5. Joho F, Novak P, Haas O, Nesper R (1993) Chimia 47:288
6. Novak P, Scheifele W, Haas O (1995) J Power Sources 54:479
7. Spahr ME, Novak P, Haas O, Nesper R (1995) J Power Sources 54:346
8. Novak P, Imhof R, Haas O (1999) Electrochim Acta 45:351
9. Makino K, Katayama Y, Miura T, Kishi T (2001) J Power Sources 99:66
10. Amatucci GG, Badway F, Singhal A, Beaudoin B, Skandan G, Bowmer T, Plitz I, Pereira N, Chapman T, Jaworskia R (2001) J Elecrochem Soc 148:A940
11. Yvon K (1979) In: Kaldis E (ed) Current topics in material science, vol 3. North-Holland Publishing Company, Amsterdam, p 53
12. Chevrel R, Sergent M, Prigent J (1974) J Mater Res Bull 9:1487
13. Schollhorn R, Kumpers M, Besenhard JO (1977) Mater Res Bull 12: 781
14. Aurbach D, Lu Z, Schechter A, Gofer Y, Gizbar H, Turgeman R, Cohen Y, Moskovich M, Levi E (2000) Nature 407:724
15. Levi MD, Lancry E, Gizbar H, Lu Z, Levi E, Gofer Y, Aurbach D (2004) J Electrochem Soc 151: A1044
16. Levi MD, Eli Lancry, Gizbar H, Gofer Y, Levi E, Aurbach D (2004) Electrochim Acta 49:3201
17. Levi MD, Gizbar H, Lancry E, Gofer Y, Levi E, Aurbach D (2004) J Electroanal. Chem 569:211
18. Levi E, Gofer Y, Vestfreed Y, Lancry E, Aurbach D (2002) Chem Mater 14:2767
19. Chusid O, Gofer Y, Gizbar H, Vestfrid Y, Levi E, Aurbach D, Riech I (2003) Adv Mater 15:627
20. Wen CJ, Boukamp BA, Huggins RA, Weppner W (1979) J Electrochem Soc 126:2258
21. Weppner W, Huggins RA (1978) Ann Rev Mater Sci 8:269
22. Levi MD, Aurbach D (1999) Electrochim Acta 45:167
23. Levi MD, Gamolsky K, Aurbach D, Heider U, Oesten R (2000) J Electrochem Soc 147:25
24. Levi MD, Wang C, Aurbach D, Chvoj Z (2004) J Electroanal Chem 562 :187